Journal of Magnetic Resonance **142,** 102–110 (2000)
Article ID jmre.1999.1907, available online at http://www.idealibrary.com on IDEAL®

^{13}C PGSE NMR Experiment with Heteronuclear Dipolar Decoupling to Measure Diffusion in Liquid Crystals and Solids

S. V. Dvinskikh,*,† R. Sitnikov,* and I. Furó,*,[1]

*Division of Physical Chemistry, Department of Chemistry, Royal Institute of Technology, SE-10044 Stockholm, Sweden; and †Institute of Physics, St. Petersburg State University, 198904 St. Petersburg, Russia

Received May 5, 1999; revised August 4, 1999

A new PGSE NMR experiment, designed to measure molecular diffusion coefficients in systems with nonvanishing static dipolar coupling, is described. The fast static dipolar dephasing of the single-quantum ^{13}C coherences is removed by multiple-pulse heteronuclear decoupling. The resulting slow dephasing of the ^{13}C coherences allows for inserting appropriate gradient pulses into the pulse sequence. The presence of the large magnetic field gradient reduces the efficiency of the decoupling sequences which is compensated for by introducing a scheme of sequential slice selection across the sample. The method is demonstrated by ^{19}F-decoupled ^{13}C PGSE NMR experiments in a lyotropic nematic and lamellar liquid crystal.

Key Words: **PGSE NMR; heteronuclear dipolar decoupling; slice selection; liquid crystals; cesium perfluorooctanoate.**

INTRODUCTION

Pulsed-field-gradient spin (or stimulated) echo (PGSE) NMR (*1–6*) is a well-established method for studying diffusive molecular motions in isotropic liquids. Conventional PGSE NMR is, however, less suitable to anisotropic liquids, such as liquid crystals, or to solids where there is only partial or no motional averaging of the dipolar interaction. In such materials, the decay of the spin coherences is fast and, of course, is not refocused by the simple spin (or stimulated) echo pulse sequence. Hence, there is usually no sufficient time to apply long and strong enough gradient pulses and the extra dephasing induced by diffusion along the applied spatial gradient of magnetic field is negligible (*7, 8*). (Important exceptions are some small, weakly ordered solutes, including water, whose weak dipole coupling allows conventional PGSE measurements (*7–9*).)

In the past, three separate avenues to diffusion coefficients in anisotropic systems were explored. The first two approaches require macroscopically oriented liquid crystal samples (or, for solids, single crystals). In the first method, the director of the oriented sample is then set to the "magic angle" with respect to the applied magnetic field (*10–13*), see also reviews (*7, 8*). Under this condition, the dipolar coupling is reduced and the connected dipolar dephasing of the coherences is prolonged. In lyotropic liquid crystals, this method has been mostly applied to lamellar phases oriented by glass plates. One drawback of this approach is its failure at phase transitions where macroscopic orientation at the magic angle is usually lost. Moreover, nematic phases which reorient quickly in the applied magnetic field cannot be measured this way. The second alternative does not require orientating the director at the magic angle, the dipolar coupling is suppressed instead by multiple-pulse averaging. Such homonuclear dipolar decoupling has been successfully combined with PGSE experiment in thermotropic and lyotropic liquid crystals (*14–16*). In the early approaches, the field gradient pulses were applied in the time windows (typically a few microseconds) between the radiofrequency (RF) pulses. This feature has necessarily limited the gradient strength and, thus, the available diffusion coefficients. Recently, multiple-pulse averaging has been combined with a large static magnetic field gradient (*17, 18*) to measure slow diffusion in plastic crystals. The third approach relies on nuclei, ^{2}H in particular, with weak dipolar and eventually strong quadrupolar interactions. The static quadrupolar interaction can be readily refocused by quadrupolar echo that is then replacing spin echo in the PGSE pulse sequence (*19–21*). The main limiting factor (beside an eventual need of deuteration) is a slow enough quadrupolar relaxation not always fulfilled by the investigated molecules.

Here we introduce a new experiment that combines *he*teronuclear *d*ipolar *d*ecoupling with PGSE (HEDD–PGSE). Our aim is to expand the range of anisotropic systems in which molecular diffusion coefficients can be measured, particularly in nematic phases, at and close phase transitions and without the need of deuteration. To do so, the NMR signal is detected on a weakly abundant nucleus, typically ^{13}C, whose sole dipolar coupling to nearby heteronuclei, such as ^{1}H or ^{19}F, is suppressed by heteronuclear decoupling. Thus, the dephasing of ^{13}C coherences is made relatively slow, allowing one to apply long and strong enough gradient pulses in the PGSE experiment. Such a combination of heteronuclear dipolar decoupling with the pulsed-field-gradient spin-echo method has

[1] To whom correspondence should be addressed. E-mail: ifuro@physchem.kth.se.

1090-7807/00 $35.00

originally been presented by Zhou and Frydman (*22, 23*). As shown below, however, their original pulse sequence is prone to large systematic errors in the obtained diffusion coefficients and to strong sample heating.

In comparison to the earlier diffusion experiments with ^{1}H homonuclear decoupling, the demands of heteronuclear decoupling on the spectrometer hardware (in particular, transmitter power) are less stringent. Moreover, heteronuclear decoupling usually leads to smaller linewidths that allow for longer gradient pulses. Artifact lines at close to zero frequency offset, caused by pulse imperfections, may be significant for homonuclear dipolar decoupling (*24*). There are no such artifacts with heteronuclear decoupling. One apparent disadvantage of our HEDD–PGSE scheme is the lower (by a factor of 4) gyromagnetic ratio of ^{13}C as compared to ^{1}H, which would make the gradient pulses less effective. One should recall, however, that homonuclear dipolar decoupling effectively lowers the frequency offset term in the average spin Hamiltonian by a pulse-sequence-dependent scaling factor (*25, 26*) (typically around 0.3–0.6); the gradient efficiency is reduced accordingly in that experiment. A significant disadvantage of the HEDD–PGSE scheme applied to natural abundance ^{13}C is the low sensitivity. As shown below, however, experiments at natural abundance are still feasible in concentrated samples. On the other hand, ^{13}C provides the advantage of its large chemical shift range with the corresponding chemical selectivity (this and some other particular advantages with ^{1}H-decoupled ^{13}C PGSE NMR in liquids have already been explored (*27, 28*)).

In this paper, we proceed as follows. First, we provide a detailed account of the new experimental procedure. Particular emphasis is laid on the relative performance of the various decoupling schemes and on the applied slice selection scheme. Then, the method is demonstrated by ^{19}F-decoupled ^{13}C PGSE NMR experiments in the nematic and lamellar phases of the lyotropic mixture of cesiumperfluorooctanoate (CsPFO)–water (*29*). As will be shown, the obtained diffusion coefficients are more accurate than the diffusion data from a previous study on the same system, but measured by ^{19}F PGSE NMR on samples with the magic angle orientation (*30*). Most importantly, we could measure within the nematic phase and close to the nematic–lamellar phase transition without any particular difficulty.

THE HEDD–PGSE METHOD

Since the longitudinal relaxation time T_1 of ^{13}C is usually rather long in liquid crystals (and in solids), the preferable choice to be combined with heteronuclear decoupling is the stimulated echo pulse sequence. Because coherence evolution periods are to be kept the shortest possible, the effect of eddy currents in the actual sequence (see Fig. 1a) is reduced via including a longitudinal eddy delay (LED) (*31*) extension. The primary function of this delay changes, however, in the new

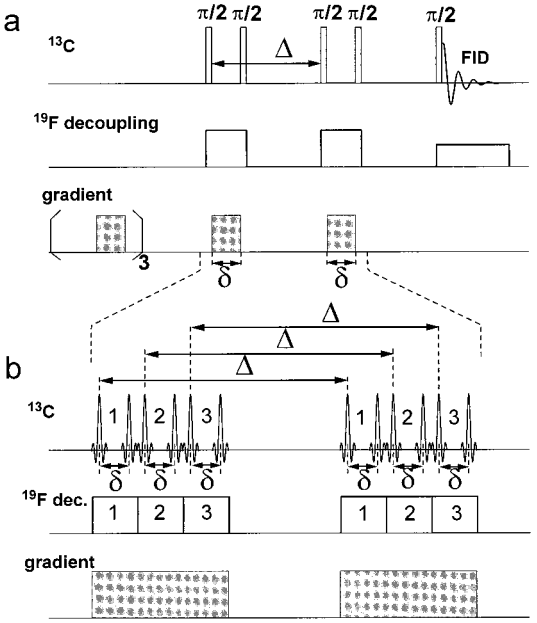

FIG. 1. (a) Conventional ^{13}C stimulated echo PGSE NMR experiment with additional LED delay and with ^{19}F heteronuclear dipolar decoupling. (b) ^{19}F-decoupled ^{13}C PGSE NMR experiment with a sequential slice selection scheme. Selective ^{13}C pulses in the presence of a field gradient excite those regions for which the ^{19}F decoupling is appropriately set. Frequency-shifted excitation and decoupling blocks, marked by numbers 1, 2, and 3, provide signals from three adjacent spatial regions. The signal components from different regions are summed as z magnetization at the beginning of the LED period. Depending on the gradient strength and decoupling bandwidth, the number of slices is adjusted to collect signal from most of the sample volume.

pulse sequence presented in Fig. 1b and introduced below. Three gradient prepulses (*31, 32*) are added as well.

One faces a particular problem when implementing heteronuclear decoupling in a diffusion experiment where efficient decoupling must be achieved during both the encoding and decoding gradient times δ (see Fig. 1). In the presence of a field gradient, different parts of the sample experience different magnetic fields, which leads to a position-dependent frequency offset across the sample volume. Thus, the selected decoupling sequence must perform effectively even at large frequency offsets. As shown below, not all dipolar decoupling designs manage this point well; in fact, even the best decoupling pulse sequences fail to decouple the ^{13}C spins in the full sample volume under the effect of the large gradients of our diffusion experiment. (This is the main reason why the straightforward combination of the conventional PGSE experiment with heteronuclear decoupling (*22, 23*) is less suitable, as demonstrated below.) One way to provide effective decoupling is to modify the probe design, e.g., to use a flat sample and a flat RF coil (*33*) with a small (~mm) extension in the gradient direction. We found this arrangement particularly unfeasible for liquid crystals whose director orientation might be distorted close to sample container wall.

Instead, we chose a more general alternative involving slice

selection, well known from magnetic resonance imaging (*4*), via selective ^{13}C pulses during the field gradient pulses. The details are depicted in Fig. 1b. First, the first four hard 90° pulses in Fig. 1a are replaced by selective pulses and the gradient pulse is extended to be on during those RF pulses. The frequencies and bandwidths of both the selective ^{13}C pulses and the ^{19}F decoupling are then adjusted so that only those regions have their ^{13}C spins excited whose heteronuclear decoupling is sufficiently effective. Finally, the frequencies of the excitation and the decoupling are stepped on a synchronous way to excite adjacent regions of the sample. In Fig. 1b, the numbers 1, 2, 3 denote the three different slices of the sample, which are excited and decoupled by the consecutive 1, 2, 3 blocks of frequency-adjusted ^{13}C and ^{19}F irradiation. The last ^{13}C selective pulse in each excitation block stores the signal as *z* magnetization; thus, contributions from all slices are conveniently summed. Finally, at the end of the LED-delay, a single hard pulse and heteronuclear decoupling (at the ^{19}F frequency of the main magnetic field) is applied to record the total signal. We note here that the use of slice selection to provide proper excitation in a large gradient has been suggested previously (*34*). It is an important difference, though, that with the LED delay at the end the pulse sequence sums the *z* magnetizations and not the FIDs from the different slices; thus, no extra spectral noise is introduced. An extra bonus of the slice selection scheme is the absence of gradient switching (and the connected eddy currents) during the encoding/decoding periods.

Care must be taken to properly adjust the ^{13}C pulse bandwidth and the ^{13}C and ^{19}F frequency offsets to avoid disturbing overlap of the selected slices. If that happened, some spins would evolve as if under the effect of a larger than nominal field gradient. Thus, in a prudent setup (that also allows for imperfections of the selective excitation profiles), slices must be kept somewhat apart which leads to unrecoverable loss of signal from the narrow, unexcited regions separating the slices. As shown below, such loss can be made small. Spins that cross the boundary of a slice between the encoding or decoding periods do not contribute to the signal. Since the typical diffusion length is in the order of μm and our slice widths were set to ~mm, this loss is negligible here.

Even with this slice selection scheme, however, diffusion experiments cannot proceed on the most usual way, i.e., by recording the variation of the signal intensity on increasing gradient strength. Impractically, the variation of the gradient would require one to correspondingly modify all the excitation and decoupling frequencies and bandwidths as well. Varying the length of delay δ is also impractical in the present setup as it would vary the heating effect from the decoupling. Thus, the only remaining option is to record the decay of the signal with increasing Δ that is described as (*2*)

$$S(\Delta) \sim \exp(-\gamma^2 g^2 \delta^2 D \Delta) \cdot \exp(-\Delta/T_1). \qquad [1]$$

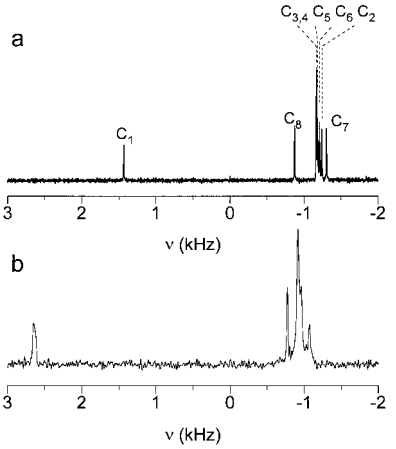

FIG. 2. ^{13}C NMR spectra of CsPFO/D_2O (at 50 wt%) in the isotropic phase at 325 K (a) and in the lamellar phase at 312 K (b), recorded at 4.7 T. FLOPSY-8 decoupling (*35, 36*) at the fluorine frequency was applied with $\gamma B_1/2\pi = 8$ kHz and $\gamma B_1/2\pi = 16$ kHz field strengths, respectively. To limit sample heating, the acquisition time (200 ms for (b)) was shortened (down to 25 ms) in the diffusion experiments.

Then, the difference between the decay constants recorded with and without gradient *g* provides one with the diffusion coefficient *D*.

One should note that the heating effects (see below) during the encoding/decoding and detection periods must be treated differently. If the waiting times between individual scans are long enough to allow the temperature gradients to disappear in-between individual scans and if one uses sufficiently many dummy scans to establish a new thermal equilibrium, systematic errors of the measured diffusion coefficient are connected solely to the heating effects (temperature shift and gradient, see Experimental) during the encoding/decoding periods. Heating by the decoupling during acquisition has only a minor influence on the detected spectral shape, but the measured diffusion coefficient is not affected. The new average temperature (that includes the average temperature shift produced by the decoupling and to which the measured diffusion coefficient can be assigned to) can be readily determined in the present test sample (see below) from the temperature sensitive ($\approx$20–40 Hz/K, depending on the temperature) ^2H quadrupole splitting (of D_2O) recorded under the same ^{19}F irradiation conditions.

RESULTS AND DISCUSSION

Spectral Features of the Test Sample

The ^{19}F-decoupled ^{13}C NMR spectra of CsPFO in D_2O, recorded at 50 MHz, are shown in Fig. 2. The isotropic liquid spectrum, recorded at 325 K and shown in Fig. 2a, is obtained with FLOPSY-8 (*35, 36*) decoupling of 8 kHz B_1 field strength. The assignment is as previously published (*37*). The residual line width of 10 Hz is mainly due to B_0 inhomogeneity which is large due to the short and horizontal sample tube. The

spectrum of the lamellar phase, recorded at 312 K and shown in Fig. 2b, is obtained with the same decoupling sequence of $\gamma B_1/2\pi = 16$ kHz. This lamellar phase is oriented (by cooling from the nematic phase) with its bilayer normal parallel to the magnetic field. The residual line width here is 30 Hz, so that carbon resonances in C_2–C_6 positions are unresolved. The carbonyl line C_1, that comes from a carbon not directly bound to fluorines, is broadened due to RF-induced temperature gradient. The frequency of this line was found to be the one most sensitive ($\sim$1.5 ppm/K) to temperature; the temperature dependence of the frequencies of the other carbons is smaller by about one order of magnitude. The relative chemical shifts of the lines C_1–C_8 are clearly different in the two spectra.

This behavior appears because the lines in the two spectra reflect different parts of a residual chemical shift anisotropy (CSA) tensor. This residual CSA tensor originates from the molecular ^{13}C CSA tensor that becomes partially averaged by fast ($\ll$ns) local motions of the surfactant chain (such as axial spinning and wobbling), in the next step by the surface diffusion of the surfactant molecule over the anisomeric aggregate (*37*), and, finally, by the tumbling of the aggregate (*21, 38*). In the isotropic micellar phase this tumbling is isotropic and the lines in Fig. 2a display the isotropic averages of the respective molecular CSA tensors. In the nematic and lamellar liquid crystal phases the tumbling is anisotropic and is characterized by the order parameter S_{aggr} connected to the orientational distribution of the aggregates. In the decoupled anisotropic spectrum (Fig. 2b), one principal value (σ_{zz}) of the residual CSA tensor is displayed. Since S_{aggr} is temperature dependent (*21*) and the residual CSA tensor is proportional to S_{aggr}, the displayed frequency shift becomes temperature dependent. Moreover, the anisotropy of the molecular CSA tensor is about one order of magnitude larger for carbonyl carbons than that for difluromethylene carbons (*25*) which explains the larger temperature sensitivity of the C_1 frequency.

Choice of the Decoupling Sequence

Adequate heteronuclear dipolar decoupling of spin S requires an RF power (field intensity) at the resonance frequency of the unobserved spin I that is in the same order as the strength of the dipolar interactions between both I–S and I–I spins. Within this range, however, the actual power demand to accomplish a good decoupling (as certified by the appearance of narrowest possible spectral lines of spin S) depends on the design of the actual decoupling pulse sequence. While a number of pulse sequences with extremely large bandwidth have been developed, most of them were specifically directed to isotropic liquids. Effective decoupling sequences for anisotropic liquids have also appeared (*39–41*). Typically, the effective decay time of ^{13}C single quantum coherences in thermotropic liquid crystals, T_2^*, has been prolonged up to tens of milliseconds by applying them at sufficiently high power levels. This last point, the required RF power, is a strong limiting factor for liquid crystal applications where material properties are strongly temperature dependent. In particular, lyotropic liquid crystals are usually highly conductive and therefore very susceptible to RF-induced heating. In principle, the average temperature shift due to this effect can be corrected for by using some temperature-dependent spectral features (see below). On the other hand, the temperature gradient within the sample cannot be dealt with on that way and should be kept at minimum.

A, perhaps minor, extra complication appears for by ^{19}F-decoupled ^{13}C NMR. As compared to C–H spin pairs in protonated compounds, C–F spins in fluorinated compounds have smaller (by about a factor of 2) dipolar and larger (by about a factor of 2) J couplings. Therefore, J couplings are not entirely negligible (although still about one order of magnitude smaller) as compared to dipolar couplings in fluorinated anisotropic liquids. Since decoupling techniques are mostly designed to suppress only one type of those interactions, they are, generally, less effective in fluorinated compounds than in protonated ones.

On the test sample presented above, we examined the performance of a wide variety of reported decoupling sequences with respect to their sensitivity to frequency offset and decoupling power. As expected, the performances of the popular composite-pulse schemes WALTZ, MLEV, GARP, DIPSI, frequency-switching sequences of MPF-family, and modern adiabatic frequency-sweeping sequences, which (see reviews (*42, 43*)) are all designed for applications in isotropic liquids, performed rather poorly in liquid crystalline phases even at zero offset. (In particular, WALTZ provided a T_2^* about one order of magnitude shorter than that achieved by COMARO-2 (*40*) or FLOPSY-8 (*35, 36*) at equal RF power, see below.) The sequence ALPHA, reported to be effective for protonated molecules dissolved in thermotropic liquid crystals (*39*), the modified phase-alternating CW-irradiation schemes TPPM (*44*), and SPARC (*41*) were all very effective in our liquid crystal phases at zero offset, but are offset sensitive by about a factor of 4 more than COMARO-2 and FLOPSY-8 (nearly as much as a simple CW decoupling).

Good results were obtained with the COMARO-2 sequence (*40*). This sequence is based on rotating the magnetization around the magic angle and is specifically designed for heteronuclear broadband decoupling in solids and liquid crystals. It gives slightly broader lines than SPARC-16, but allows a much wider frequency offset range. Somewhat surprisingly, however, the best performance was shown by the FLOPSY-8 sequence which originally was developed for broadband homonuclear cross polarization (*35, 36*). We found that FLOPSY-8 outperforms COMARO-2 in the frequency offset range by a factor of $\approx$2 at equal RF power, gives virtually the same resolution, and is very stable with respect to miscalibration of the 90° pulse. Hence, we decided to use FLOPSY-8 for decoupling during the gradient encoding and decoding periods,

while either FLOPSY-8 or SPARC-16 for signal acquisition (see Fig. 1b).

Even with the best decoupling sequence, however, we were forced to use rather high decoupling power (see below). This has lead to significant heating in our ionic and therefore highly dissipative sample even though steps (like using flat wire in and limiting the diameter of the RF coil to 6 mm and the number of turns to 8 (*45*), see Experimental) were taken to reduce this problem. With on-resonance decoupling, reasonably narrow lines were achieved with a decoupling field strength of $\gamma B_1/2\pi = 16$ kHz. Further increase of B_1 up to 25 kHz improved the resolution somewhat, but has not been used because of excessive (see Experimental) heating; note that RF heating is proportional to $(B_1)^2$ (*45*). To decouple during the relatively short encoding/decoding periods a slightly higher RF field of $\gamma B_1/2\pi = 20$ kHz was used to get a longer T_2^* and a wider frequency offset range. At the cited field strengths we observed no coil arcing or preamplifier and transmitter overload.

Diffusion Measurement with HEDD–PGSE

The first test of the HEDD–PGSE experiment of Fig. 1, performed on benzene at 25°C, assessed the validity of this experimental approach. ^{1}H-decoupled ^{13}C PGSE experiments yielded a large signal from the six equivalent carbons, allowing relatively quick and accurate measurements of the fast benzene diffusion coefficient. As indicated in Fig. 1, delays δ and Δ were defined by the centers of the selective pulses whose 400 μs full length provided (for their truncated sinc shape) a nominal bandwidth of 15 kHz. The results were compared to $D_{benzene}$ obtained from a conventional hard pulse ^{13}C PGSE NMR experiment. If δ exceeded 4 ms, the results coincided within the experimental accuracy of 2%. For shorter δ's, systematic errors, probably connected to dephasing during the RF pulses of nonnegligible length, appeared. For $\delta = 2$ and 1 ms, the obtained diffusion coefficients were larger by 5 and 15%, respectively, than $D_{benzene}$. First, this systematic error could be largely corrected for, if necessary, in Eq. [1] by exactly calculating the joint effect of the selective RF pulses and the gradient fields. Second, experiments with short δ can be still valuable in the frequently occurring experimental situation when one is primarily interested in the relative change of a diffusion coefficient. In another test, no difference within experimental error was found between the diffusion coefficients obtained from experiments with the sample volume divided into one, two, or three slices.

The diffusion coefficient of CsPFO in the lamellar phase of our present sample composition has already been measured and the value obtained in the direction perpendicular to the external static magnetic field is $D_\perp \approx 10^{-10}$ m^2/s (*30*). Note that the lamellar phase orients with its bilayer normal parallel to the magnetic field; thus, $D_\perp$ is the surfactant diffusion coefficient along the (defective) bilayers. ($D_\parallel$, which measures the diffusion coefficient perpendicular to the bilayers, was shown to be much lower than $D_\perp$ and is probably connected to exchange of individual surfactant molecules between adjacent bilayers.) From the known values of $D_\perp$ and of the T_2^* and T_1 times one can estimate the gradient strength, required to measure $D_\perp$ by the HEDD–PGSE experiment, to $g \geq 100$ G/cm. Such gradients lead to a fluorine offset distribution of $\geq$160 kHz in our sample of 4 mm diameter. Despite good performance of the FLOPSY decoupling, this offset range is too wide to excite; at $B_1 = 20$ kHz, sufficiently good decoupling was observed in the fluorine offset range of about 50 kHz (determined as the offset where line intensity decreases by a factor of two with respect to zero offset). Indeed, we had to apply the sequential slice selection as shown in Fig. 1b.

Below we present the actual experimental setup optimized for the gradient value $g = 114$ G/cm, where the fluorine and carbon frequency offset distributions are 180 and 48 kHz wide, respectively. Thus, one can select three slices, each with fluorine decoupling effective in the offset range of approximately 50 kHz. Correspondingly, the selective ^{13}C pulses were defined to provide 15 kHz nominal excitation bandwidth. To avoid interference between neighboring slices (due to "wings" of the excitation and decoupling profiles), the three central offset frequencies of the ^{13}C excitation packages were set to -17, 0, and $+17$ kHz (0 kHz belongs to the middle of the sample). The frequency offsets for ^{19}F decoupling were set to -64, 0, and $+64$ kHz, respectively. This arrangement provides 2 kHz wide gaps (in ^{13}C frequencies) to separate the slices. Under these conditions we recover approximately 75% of the ^{13}C signal intensity which can be compared to the 30% signal intensity achieved with the conventional hard pulse experiment of Fig. 1a (100% defines the signal intensity at zero gradient; see Experimental). In fact, 2 kHz wide gaps maximize the signal; smaller gaps also lead to signal reduction. The 25% signal loss is partly connected to the unexcited gap, partly to the smoothly decaying (instead of having sharp edges) ^{19}F decoupling profile.

The results of the HEDD–PGSE experiments in the lamellar phase of CsPFO/D_2O are shown in Fig. 3, with signal intensities plotted versus the mixing time Δ in semilogarithmic scale. Several decays obtained at different field gradients, all applied perpendicularly to the B_0 field, are presented. δ was fixed to 2 ms, chosen to be much shorter than the effective transverse relaxation time estimated to $T_2^* \approx 7$ ms (the average value for C_2–C_8 lines at 114 G/cm gradient strength). Although the experiments with lower gradient manage with fewer slices, all experiments were performed with the same pulse sequence to ensure equivalent conditions. For each point 256 scans were accumulated, so that one decay curve took approximately 16 h of the experimental time (see Experimental; shorter recycle times currently allow 8 h experimental time, with still negligible heating effects). The lines in Fig. 3 are the single exponential fits to the experimental points; obviously, the decays are single-exponential within the experimental accuracy. (In

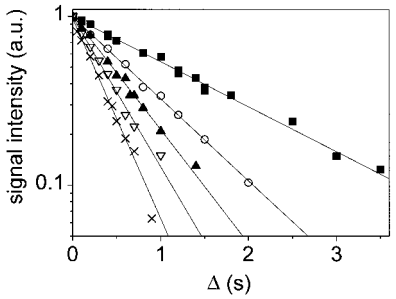

FIG. 3. Variation of the signal intensity with increasing the delay time Δ in the PGSE experiment depicted in Fig. 1b, applied in lamellar phase of CsPFO/D_2O (50 wt%) at 312 K. The liquid crystal sample is uniformly oriented by the magnetic field with its director parallel to the field direction. The magnetic field gradient g is applied perpendicularly to the field direction. The symbols represent data recorded at different field gradient values and the lines are single exponential fits as described by Eq. [1]. The fitted decay rates $R = (\gamma^2 g^2 \delta^2 D + 1/T_1)$ are as follows. (■) $g = 0$ G/cm, $R = 0.61 \pm 0.01$ s^{-1}; (○) $g = 57$ G/cm, $R = 1.12 \pm 0.02$ s^{-1}; (▼) $g = 76$ G/cm, $R = 1.55 \pm 0.04$ s^{-1}; (Δ) $g = 95$ G/cm, $R = 2.05 \pm 0.06$ s^{-1}; (×) $g = 114$ G/cm, $R = 2.73 \pm 0.07$ s^{-1}.

the micellar phase, the longitudinal relaxation rates of different carbons C_2–C_8 are rather similar (*37*), which explains why the composite decay with $g = 0$ is close to single-exponential.)

The validity of Eq. [1] is demonstrated in Fig. 4, where the expected linear dependence of the decay constant on g^2 is clearly manifested. The error bars in Fig. 4 (typically ±2%) are probable standard deviations provided by the fit statistics. Obviously, the linearity of Fig. 4 means that the diffusion coefficients derived from the measurements at different gradient strengths agree well. The explicit value of the diffusion coefficient is obtained as the difference of the rate constants in measurements with and without gradient. For $D_\perp$ at 312 K, we thus get $(0.90 \pm 0.02) \times 10^{-10}$ m^2/s. Note that the absolute value of this diffusion coefficient may contain an error of about 5% as estimated from the tests in liquid benzene (see above). For comparison, we also measured $D_\parallel$ that is expected to be much smaller; we obtain $(0.070 \pm 0.025) \times 10^{-10}$ m^2/s. Finally, $D_\perp$ was measured at several different temperatures and within both the nematic and the lamellar phases; the results are collected in Fig. 5. The results in lamellar phase are in a reasonable agreement with the ^{19}F PGSE diffusion measurements at the magic angle orientation by Ukleja *et al.* (*30*), although in that study the diffusion coefficient was not established close to the phase transition temperature.

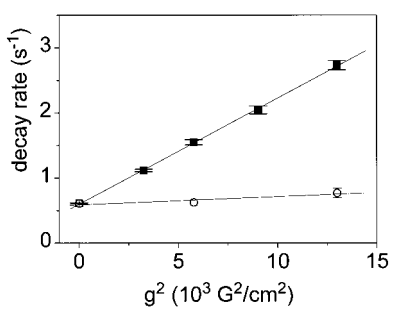

FIG. 4. Decay rates R as obtained from the data in Fig. 3 versus g^2 (■). The data display a linear dependence as expected from Eq. [1]. Some decay rates from the same sample but measured with gradients parallel (○) to the static magnetic field are presented as well; the diffusion is slower in the latter direction.

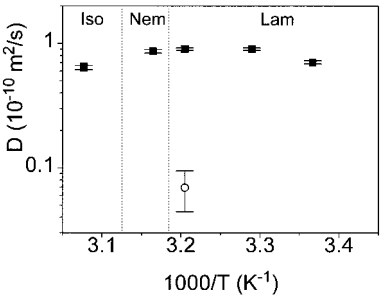

FIG. 5. The temperature dependence of the diffusion coefficient $D_\perp$ (■) in the CsPFO/D_2O system. $D_\parallel$ (○) measured in lamellar phase at 312 K is also shown.

Comparison of the HEDD–PGSE and the Zhou–Frydman Type (22, 23) Experiment

In this section we analyze the performance of the method that straightforwardly combines heteronuclear decoupling with PGSE-type diffusion experiments. In their original paper, Zhou and Frydman (*22, 23*) used the spin-echo pulse sequence that is excluded in our sample since the ^{13}C transverse relaxation time T_2^* is prohibitively short. Instead, we compare the performance of the simple stimulated echo pulse sequence (Fig. 1a) to that of HEDD–PGSE (Fig. 1b). As in (*22, 23*), we record the decay of the signal with increasing gradient strength. In (*22, 23*) the decoupling has been achieved by WALTZ which, however, provides us with $T_2^* \approx 1$ ms (at 20 kHz decoupling strength). Hence, the ^{19}F nuclei are decoupled instead by FLOPSY-8 during the encoding and decoding periods. The conditions are the same as for the HEDD–PGSE study above and the delays in the pulse sequence were set to $\delta = 2$ ms and $\Delta = 100$ ms.

The data in Fig. 6a were obtained with decoupling at 20 kHz. With on-resonance decoupling, this provides $T_2^* \approx 10$ ms and the heating effect from the decoupling during encoding/decoding and acquisition periods is below 1 K. The data were obtained at parallel and perpendicular orientations of the field gradient to the liquid crystal director (which is oriented along the static magnetic field). The expected decays at these two gradient directions, as calculated from the diffusion coefficients $D_\perp = 0.90 \times 10^{-10}$ and $D_\parallel = 0.07 \times 10^{-10}$ m^2/s obtained by HEDD–PGSE above, are also presented. (We stress that our $D_\perp$ and $D_\parallel$ data agree well with those obtained by ^{19}F PGSE experiments in samples oriented at the magic angle (*30*).)

First, the experimental decay is clearly non-Gaussian. Sec-

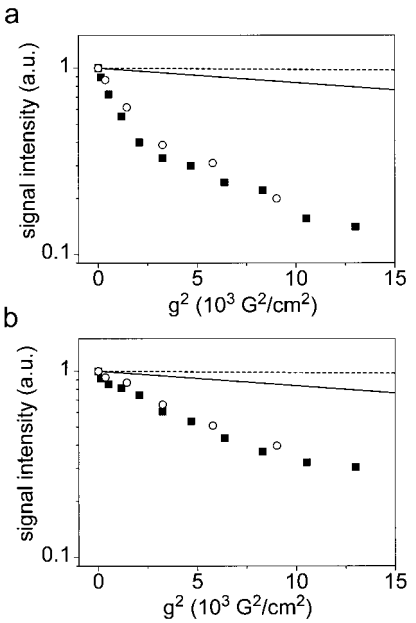

FIG. 6. Decays of the observed signal with increasing gradient strength in the simple stimulated echo experiment (*22*) without the slice selection scheme and with FLOPSY-8 decoupling in the lamellar phase at 312 K. The strength of the decoupling field $\gamma B_1/2\pi$ is (a) 20 and (b) 40 kHz. Open and full symbols belong to gradients parallel and perpendicular to B_0, respectively. Theoretical decay curves calculated from the experimental diffusion coefficients (see $D_\perp$ and $D_\parallel$ in Fig. 5) under the assumption of diffusion-dominated decays are presented as solid ($D_\perp$) and dashed ($D_\parallel$) lines.

ond, fitting the data to the conventional Stejskal–Tanner expression (*2*) gives the apparent diffusion coefficient of 30×10^{-10} m^2/s for both gradient directions. Increasing the strength of the decoupling field during encoding/decoding time to 40 kHz leads to significant prolongation of the measured decays (Fig. 6b) and to an apparent diffusion coefficient of 13×10^{-10} m^2/s. Obviously, even at this intensity of the decoupling RF field the observed decay cannot be attributed to molecular diffusion. Instead, the decay reflects the decreasing efficiency of the decoupling as the increasing gradient renders various parts of the sample further and further off-resonance. In our sample, one would need a further order of magnitude increase of the decoupling power to avoid this artifact. Of course, the sample would be heated by about 50–100 K.

To overcome this problem in the design of (*22*), one could try to accelerate the diffusion decay within the same range of field gradient by further increasing the gradient time δ and/or the diffusion time Δ. The first problem with that approach is the great loss of the signal-to-noise ratio (that is already the most critical point of the experiment). Nevertheless, data (not shown) obtained with $\delta = 6$ ms and $\Delta = 500$ ms (which are now comparable with the T_2^* and T_1 times, respectively) and with 20 kHz decoupling strength provide diffusion coefficients that are still overestimated by a factor of two ($D_\perp$) and by a factor of 13 ($D_\parallel$). In summary, the method presented in (*22*) is not suitable to measure molecular diffusion in our or in similar lyotropic liquid crystal systems. In its original presentation, the method has been applied to a thermotropic liquid crystal with long T_2^*. We note that some of the obtained results, such as the decreasing anisotropy of the diffusion with decreasing temperature (*22*), are counterintuitive.

CONCLUSION

In this paper, we propose and demonstrate a method for measuring the molecular diffusion coefficients in systems with strong static dipolar interactions. The method, as presented, is specifically optimized to investigate self-diffusion in liquid crystals. While it is relatively straightforward to apply heteronuclear decoupling to prolong the decay times T_2^* of the ^{13}C single-quantum coherences, the inherent offset dependence of the decoupling efficiency must be countered by combining the PGSE experiment with slice selection. The results clearly demonstrate that diffusion coefficients down to 10^{-12}–10^{-11} m^2/s can be readily measured in systems with strong static dipolar couplings. The implementation of the method is not difficult and at most requires double-tuning of the RF part of a standard diffusion probe. Extra care should be taken, however, to avoid RF heating effect in conductive samples. Coil designs optimized for the minimum electric field (*46, 47*) can turn out to be advantageous.

Clearly, the measurement takes considerable time because of the low ^{13}C abundance. Again, this problem is much related to sample heating and the corresponding long waiting times between scans. Further work is in progress to alleviate this problem. In some systems, however, there are simply no other options to measure diffusion. Such is our choice for demonstrating the method, the sequence of the CsPFO/D_2O liquid crystal phases. The nature of the phase transitions shown by this material is unclear, the extent and onset of the topological changes of the surfactant aggregates is an unanswered question (*21, 48–52*). Surfactant diffusion coefficients are ideally suited to provide some answers, but previously they were only available in the lamellar and the isotropic phases and even there not in the vicinity of the phase transition temperatures. This shortcoming is remedied here and the surfactant diffusion coefficient in the nematic phase, presented in Fig. 5, is, to our knowledge, the first of its kind in lyotropic liquid crystals. One preliminary conclusion we can draw from the data is that the defect density in the lamellar phase is clearly decreasing between 2 and 10 K below the nematic–lamellar phase transition. More detailed data on the present and on other liquid crystals will be communicated elsewhere.

EXPERIMENTAL

Cesium perfluorooctanoate CsPFO has been synthesized as described previously (*21*). The liquid crystal sample has been produced by mixing CsPFO (50 wt%) with D_2O. The isotropic–nematic and nematic–lamellar phase transition tempera-

tures were established from the ^2H spectrum to 320 and 314 K, respectively, which agree well with those of the previously established phase diagram (*29*). The nematic phase director orients parallel to the external magnetic field and keeps oriented while cooling to the lamellar phase (*53*).

The measurements were performed on a Bruker DMX 200 spectrometer, operating at 50 MHz for ^{13}C. We used a home-built probe whose exchangeable gradient setup includes quadrupole gradient coils with gradient directions parallel or perpendicular to the static magnetic field as described previously (*20*). Note that the gradient directions (x and z) are radial for the cylindrical sample space. The RF part of the probe has been rebuilt to allow triple frequency ^2H–^{13}C–^{19}F excitation with a single 6-mm i.d. and 2-cm long RF solenoid, made of 8 turns of flat wire. The lengths of the ^{13}C and ^{19}F 90° pulses were 7 μs (with 150 W irradiation power) and 10 μs (with 75 W irradiation power), respectively. The sample resided in a 5-mm o.d. and 15-mm long sealed glass ampule. The gradient coils were driven by Bruker BAFPA-40 current generators. The current in the present experiments did not exceed 3 A. ^{19}F–^{13}C Hartmann–Hahn cross polarization (in the lamellar phase) or NOE (in the nematic and isotropic phases) was applied (not shown in Fig. 1) to enhance the ^{13}C signal intensity. The selective sinc-shaped RF pulses (Fig. 1b) were truncated at the third zero crossing on either side. A routine phase cycle (1st pulse: $+x$, $-x$; 2nd and 3rd pulses: $2(+x)$, $2(+y)$, $2(-x)$, $2(-y)$; 4th and 5th pulses: $8(+x)$, $8(-x)$; receiver: $+x$, $2(-x)$, $2(+x)$, $2(-x)$, $+x$) was applied to filter out signal coming from unwanted coherence transfer pathways. (These unwanted pathways are, for nonzero gradient, cancelled by the gradient. Hence, for an on-resonant line and with zero gradient, the intensity obtained by our stimulated echo sequence is half of the intensity that would be obtained without applying any phase cycle.) The gradient strength was calibrated by measuring the diffusion coefficient of benzene at 25°C and comparing that to the literature value $D = 2.207 \times 10^{-9}$ m^2/s (*54*).

Up to 256 transients (preceded by 16 dummy scans) were accumulated for each individual spectra of the diffusion experiment. The signal intensities recorded in Fig. 3 are full integral intensities of the C_2–C_8 spectral region. The average temperature was observed and regulated with an accuracy of 0.1 K by the Bruker BVT-3000 unit supplied with the spectrometer. Temperature shift and temperature gradient within the sample caused by the RF irradiation for ^{19}F decoupling was calibrated by observing the splitting and broadening of the temperature-sensitive ^2H NMR spectra (*29*) of D_2O in the sample. In the diffusion experiments, a recycle delay of 20 s (much longer than required for full spin relaxation) was used to allow for sufficient heat dissipation from the RF irradiation for heteronuclear decoupling. At the end of the recycle delay, the average temperature spread within the sample volume was less than 0.2 K. Heating effects during the encoding/decoding period amount to about 0.2 K average temperature spread and about 0.2 K average temperature shift. The average temperature shift due to decoupling during the acquisition time was about 0.3 K. These temperature shifts were not corrected for in this study.

ACKNOWLEDGMENTS

This work has been supported by the Swedish Research Council for Engineering Sciences (TFR), the Carl Tryggers Foundation, and the Swedish Natural Science Research Council (NFR). S.D. thanks the Royal Swedish Academy (KVA) for a scholarship.

REFERENCES

1. E. O. Stejskal and J. E. Tanner, Spin diffusion measurements: Spin echoes in the presence of a time-dependent field gradient, *J. Chem. Phys.* **42,** 288–292 (1965).
2. J. E. Tanner, Use of the stimulated echo in NMR diffusion studies, *J. Chem. Phys.* **52,** 2523–2526 (1970).
3. P. Stilbs, Fourier transform pulsed-gradient spin-echo studies of molecular diffusion, *Prog. Nucl. Magn. Reson. Spectrosc.* **19,** 1–45 (1987).
4. P. T. Callaghan, "Principles of Nuclear Magnetic Resonance Microscopy," Clarendon Press, Oxford (1991).
5. W. S. Price, Pulsed-field gradient nuclear magnetic resonance as a tool for studying translational diffusion: Part I. Basic theory, *Concepts Magn. Reson.* **9,** 299–336 (1997).
6. W. S. Price, Pulsed-field gradient nuclear magnetic resonance as a tool for studying translational diffusion: Part II. Experimental aspects, *Concepts Magn. Reson.* **10,** 197–237 (1998).
7. G. J. Krüger, Diffusion in thermotropic liquid crystals, *Phys. Rep.* **82,** 229–269 (1982).
8. G. Lindblom and G. Orädd, NMR studies of translational diffusion in lyotropic liquid crystals and lipid membranes, *Progr. NMR Spectrosc.* **26,** 483–515 (1994).
9. M. E. Moseley and A. Loewenstein, Anisotropic translational diffusion of methane and chloroform in thermotropic and smectic liquid crystals, *Mol. Cryst. Liq. Cryst.* **90,** 117–144 (1982).
10. G. J. Krüger, H. Spiesecke, and R. Weiss, A simple spin echo measurement of the anisotropy of the self-diffusion coefficient in a smectic A and B type liquid crystal, *Phys. Lett. A* **51,** 295–296 (1975).
11. G. J. Krüger, H. Spiesecke, R. V. Steenwinkel, and F. Noack, Nuclear magnetic relaxation and self diffusion in a series of p-alkanoyl-benzylidene-p′-aminoazobenzenes, *Mol. Cryst. Liq. Cryst.* **40,** 103–116 (1977).
12. S. B. W. Roeder, E. E. Burnell, A. L. Kuo, and C. G. Wade, Determination of the lateral diffusion coefficient of potassium oleate in the lamellar phase, *J. Chem. Phys.* **64,** 1848–1849 (1976).
13. G. Lindblom and H. Wennerström, Amphiphile diffusion in model membrane systems studied by pulse NMR, *Biophys. Chem.* **6,** 167–171 (1977).
14. R. Blinc, J. Pirs, and I. Zupancic, Measurement of self-diffusion in liquid crystals by a multiple-pulse NMR method, *Phys. Rev. Lett.* **30,** 546–549 (1973).
15. M. S. Crawford, B. C. Gerstein, A. L. Kuo, and C. G. Wade, Diffusion in rigid bilayer membranes. Use of combined multiple pulse and multiple pulse gradient techniques in nuclear magnetic resonance, *J. Am. Chem. Soc.* **102,** 3728–3732 (1980).
16. J. Stepisnik, Analysis of NMR self-diffusion measurements by a density matrix calculation, *Physica B* **104,** 350–364 (1981).
17. I. Chang, G. Hinze, G. Diezemann, F. Fujara, and H. Sillescu,

Self-diffusion coefficient in plastic crystals by multiple-pulse NMR in large static field gradients, *Phys. Rev. Lett.* **76,** 2523–2526 (1996).

18. I. Chang, G. Diezemann, G. Hinze, R. Böhmer, and H. Sillescu, Far-off-resonance averaging of dipolar interactions in solids, *J. Magn. Reson.* **124,** 165–171 (1997).
19. P. T. Callaghan, M. A. Le Gros, and D. N. Pinder, The measurement of diffusion using deuterium pulsed field gradient nuclear magnetic resonance, *J. Chem. Phys.* **79,** 6372 (1983).
20. I. Furó and H. Jóhannesson, Accurate anisotropic water diffusion measurements in liquid crystals, *J. Magn. Reson. A* **119,** 15–21 (1996).
21. H. Jóhannesson, I. Furó, and B. Halle, Orientational order and micelle size in the nematic phase of the cesium pentadecafluorooctanoate-water system from the anisotropic self-diffusion of water, *Phys. Rev. E* **53,** 4904–4917 (1996).
22. M. Zhou and L. Frydman, Pulsed-gradient spin-echo measurements of anisotropic diffusion by dipole-decoupled ^{13}C nuclear magnetic resonance, *Solid State Nucl. Magn. Reson.* **4,** 301–307 (1995).
23. M. Zhou, V. Frydman, and L. Frydman, NMR analyses of order and dynamics in poly(p-benzamide)/sulfuric acid solutions, *Macromolecules* **30,** 5416–5428 (1997).
24. W. K. Rhim, D. D. Elleman, L. B. Schreiber, and R. W. Vaughan, Analysis of multiple pulse NMR in solids. II, *J. Chem. Phys.* **60,** 4595–4604 (1974).
25. M. Mehring, "Principles of High Resolution NMR in Solids," Springer, Berlin (1983).
26. D. P. Burum, M. Linder, and R. R. Ernst, Low-power multi-pulse line narrowing in solid-state NMR, *J. Magn. Reson.* **44,** 173–188 (1981).
27. P. Stilbs and M. E. Moseley, Carbon-13 pulsed-gradient spin-echo studies, a method for the elimination of J-modulation and proton exchange effects in self-diffusion measurements, *Chem. Scr.* **15,** 215–216 (1980).
28. P. Stilbs, Molecular self-diffusion coefficients in Fourier transform nuclear magnetic resonance spectrometric analysis of complex mixtures, *Anal. Chem.* **53,** 2135–2137 (1981).
29. N. Boden, S. A. Corne, and K. W. Jolley, Lyotropic mesomorphism of the cesium pentadecafluorooctanoate/water system: High-resolution phase diagram, *J. Phys. Chem.* **91,** 4092–4105 (1987).
30. P. Ukleja, G. Chidichimo, and P. Photinos, Pulsed gradient NMR study of anisotropic surfactant diffusion in the caesium perfluoro octanoate/D_2O system, *Liquid Cryst.* **9,** 359–367 (1991).
31. S. J. Gibbs and C. S. Johnson, A PFG NMR experiment for accurate diffusion and flow studies in the presence of eddy currents, *J. Magn. Reson.* **93,** 395–402 (1991).
32. E. v. Meerwall and M. Kamat, Effect of residual field gradients on pulsed-gradient NMR diffusion measurements, *J. Magn. Reson.* **83,** 309–323 (1989).
33. B. Bechinger and S. J. Opella, Flat-coil probe for NMR spectroscopy of oriented membrane samples, *J. Magn. Reson.* **95,** 585–588 (1991).
34. R. Kimmich and E. Fischer, One- and two-dimensional pulse sequences for diffusion experiments in the fringe field of superconducting magnets, *J. Magn. Reson. A* **106,** 229–235 (1994).
35. M. Kadkhodaie, O. Rivas, M. Tan, A. Mohebbi, and A. J. Shaka, Broadband homonuclear cross polarization using flip-flop spectroscopy, *J. Magn. Reson.* **91,** 437–443 (1991).
36. T. L. Hwang, M. Kadkhodaei, A. Mohebbi, and A. J. Shaka, Coherent and incoherent magnetization transfer in the rotating frame, *Magn. Reson. Chem.* **30,** S24–S34 (1992).
37. I. Furó and R. Sitnikov, Order parameter profile of perfluorinated chains in a micelle, *Langmuir* **15,** 2669–2673 (1999).
38. I. Furó and B. Halle, Micelle size and orientational order across the nematic-isotropic phase transition: A field-dependent nuclear-spin-relaxation study, *Phys. Rev. E* **51,** 466–477 (1995).
39. B. M. Fung, D. S. L. Mui, I. R. Bonnell, and E. L. Enwall, Evaluation of broadband decoupling sequences applied to liquid crystal solutions, *J. Magn. Reson.* **58,** 254–260 (1984).
40. K. V. Schenker, D. Suter, and A. Pines, Broadband heteronuclear decoupling in the presence of homonuclear dipolar and quadrupolar interactions, *J. Magn. Reson.* **73,** 99–113 (1987).
41. Y. Yu and B. M. Fung, An efficient broadband decoupling sequence for liquid crystals, *J. Magn. Reson.* **130,** 317–320 (1998).
42. A. J. Shaka, Decoupling methods, *in* "Encyclopedia of Nuclear Magnetic Resonance" (D. M. Grant and R. K. Harris, Eds.) pp. 1558–1564, Wiley, New York (1996).
43. R. Freeman, "Spin Choreography," Spektrum, Oxford (1997).
44. A. E. Bennett, C. M. Rienstra, M. Auger, K. V. Lakshmi, and R. G. Griffin, Heteronuclear decoupling in rotating solids, *J. Chem. Phys.* **103,** 6951–6958 (1995).
45. D. I. Hoult and P. C. Lauterbur, The sensitivity of the zeugmatographic experiment involving human samples, *J. Magn. Reson.* **34,** 425–433 (1979).
46. D. W. Alderman and D. M. Grant, An efficient decoupler coil design which reduces heating in conductive samples in superconducting spectrometers, *J. Magn. Reson.* **36,** 447–451 (1979).
47. G. J. Kost, S. E. Anderson, G. B. Matson, and C. B. Conboy, A cylindrical-window NMR probe with extended tuning range for studies of the developing heart, *J. Magn. Reson.* **82,** 238–252 (1989).
48. N. Boden, S. A. Corne, M. C. Holmes, P. H. Jackson, D. Parker, and K. W. Jolley, Order-disorder transitions in solutions of discoid micelles, *J. Phys. (Paris)* **47,** 2135–2144 (1986).
49. M. C. Holmes, D. J. Reynolds, and N. Boden, Concentration–temperature dependence of the size and shape of the micelles in the cesium pentadecafluorooctanoate/water system, *J. Phys. Chem.* **91,** 5257–5262 (1987).
50. N. Boden, Micellar liquid crystals, *in* "Micelles, Membranes, Microemulsions, and Monolayers" (W. M. Gelbart, A. Ben-Shaul, and D. Roux, Eds.) pp. 153–218, Springer, New York (1994).
51. M. C. Holmes, M. S. Leaver, and A. M. Smith, Nematic and disrupted lamellar phases in cesium pentadecafluorooctanoate/^2H_2O: A small angle scattering study, *Langmuir* **11,** 356–365 (1995).
52. G. Fröba and J. Kalus, Structure of the isotropic, nematic, and lamellar phase of a solution of tetramethylammonium perfluorononanoate in D_2O, *J. Phys. Chem.* **99,** 14,450–14,467 (1995).
53. N. Boden, G. R. Hedwig, M. C. Holmes, K. W. Jolley, and D. Parker, Anomalous effects in experiments on monodomain nematic and lamellar phases of the caesium pentadecafluoroocatnoate (CsPFO)/water system, *Liq. Cryst.* **11,** 311–324 (1992).
54. M. Holz and H. Weingärtner, Calibration in accurate spin-echo self-diffusion measurements using ^1H and less-common nuclei, *J. Magn. Reson.* **92,** 115–125 (1991).